J Mol Model (2008) 14:891–899
DOI 10.1007/s00894-008-0340-x

ORIGINAL PAPER

Homology modeling and dynamics of the extracellular domain of rat and human neuronal nicotinic acetylcholine receptor subtypes α4β2 and α7

William H. Bisson · Gerrit Westera · P. Augustus Schubiger · Leonardo Scapozza

Received: 28 March 2008 / Accepted: 13 June 2008 / Published online: 8 July 2008

Abstract In recent years, it has become clear that the neuronal nicotinic acetylcholine receptor (nAChR) is a valid target in the treatment of a variety of diseases, including Alzheimer's disease, anxiety, and nicotine addiction. As with most membrane proteins, information on the three-dimensional (3D) structure of nAChR is limited to data from electron microscopy, at a resolution that makes the application of structure-based design approaches to develop specific ligands difficult. Based on a high-resolution crystal structure of AChBP, homology models of the extracellular domain of the neuronal rat and human nAChR subtypes α4β2 and α7 (the subtypes most abundant in brain) were built, and their stability assessed with molecular dynamics (MD). All models built showed conformational stability over time, confirming the quality of the starting 3D model. Lipophilicity and electrostatic potential studies performed on the rat and human α4β2 and α7 nicotinic models were compared to AChBP, revealing the importance of the hydrophobic aromatic pocket and the critical role of the α-subunit Trp—the homolog of AChBP-Trp 143—for ligand binding. The models presented provide a valuable framework for the structure-based design of specific α4β2 nAChR subtype ligands aimed at improving therapeutic and diagnostic applications.

Keywords Nicotinic acetylcholine receptor · Homology modeling · Molecular dynamics · Hydrophobic and electrophilic potentials · Subtype selectivity

W. H. Bisson · G. Westera · P. A. Schubiger
Center for Radiopharmaceutical Sciences, Paul Scherrer Institute, Villigen and University Hospital of Zürich,
Swiss Federal Institute of Technology Zurich,
Ramistrasse 100,
8091 Zurich, Switzerland

L. Scapozza
Pharmaceutical Biochemistry Group,
School of Pharmaceutical Sciences, University of Geneva,
24 rue du General-Dufour,
1211 Geneva, Switzerland

Present address:
W. H. Bisson (✉)
The Scripps Research Institute,
10550 North Torrey Pines Rd,
La Jolla, CA 92037, USA
e-mail: wbisson@scripps.edu

Introduction

Ion channels are membrane proteins with an important physiological and pharmacological role. The nicotinic acetylcholine receptor (nAChR), a member of the Cys-loop superfamily, is a ligand-gated ion channel located mostly in the central and peripheral nervous system and neuromuscular junctions. In particular, neuronal nAChRs are present in presynaptic regions to mediate acetylcholine neurotransmission, and in the postsynaptic membrane to propagate the nerve pulse, via acetycholine, through the neurons [1]. The nAChR is composed of five subunits, which form a cation-permeable pore built up of homopentamers or heteropentamers. The binding sites are located at the interface between the two extracellular subunits, and the number of binding sites differs from subtype to subtype [2]. Thus, different nAChR subtypes exist according to the type of α and β-subunit composition. Opening of the channel can be caused by agonists other than acetylcholine, like nicotine or epibatidine [3], or by synthetic compounds [4]. Reconstitution experiments performed in host systems such as *Xenopus laevis* oocytes, and/or transfection in cell lines in

combination with site-directed mutagenesis and single-channel studies have been performed. The results of reconstitution experiments have demonstrated that the pentameric assemblies $(\alpha4)_2(\beta2)_3$ and $(\alpha7)_5$ are the subtype most abundant in the brain [5]. In addition, the identification of many neuronal nAChR genes has provided new insights into the mechanisms of neurotransmission that correlate neurological diseases and nAChRs [6]. In the last few years, neuronal nAChRs have become an important drug target for a variety of diseases, including Alzheimer's disease [4].

Considerable effort has been made to investigate and understand the structure of nAChRs, especially in the binding site region. Due to problems with crystallization, as is the case for most membrane proteins, the only available three-dimensional (3D) structural information for nAChRs involving both the extracellular ligand binding domain (LBD) and the transmembrane domain (TMD) is some low-resolution electron microscopy data from the electric organ of the *Torpedo* ray [7, 8].

High-resolution crystallographic structures of the homopentameric acetylcholine-binding protein (AChBP) isolated from the freshwater snail *Lymnaea stagnalis*, have revealed important information regarding activated and desensitized nAChR-LBD [9–13]. This protein is produced and stored in glia cells and released into the synaptic cleft in an acetylcholine-dependent manner to modulate neurotransmission. AChBP binds nAChR agonists such as acetylcholine, nicotine and the competitive antagonist α-bungarotoxin, and exhibits significant sequence homology with the extracellular part of nAChR subunits (26% identity with subtype α7) [14]. Moreover, AChBP exhibits pharmacological properties and ligand affinities similar to those of the α7 homopentamer, suggesting 3D structural similarities [15–17]. Therefore, AChBP is a suitable template 3D-structure for the N-terminal domain of nAChR α and β subunits.

In recent years, interesting structural investigations into human nAChR subtype α7 showed, through molecular dynamics (MD), important 3D-correlations during the opening and closing of the ion channel between the extracellular LBD and the TMD of the membrane protein [18–22]. Recently, the role of water in the AChBP binding pocket has also been taken into consideration [23].

In the present work, homology models of the extracellular domain of neuronal rat and human nAChR subtypes $(\alpha4)_2(\beta2)_3$ and $(\alpha7)_5$ were built, their stability assessed using MD, and the binding sites analyzed and compared regarding lipophilicity and electrostatic potential. The present models provide a valuable framework for the structure-based design of specific α4β2 nAChR subtype ligands for future therapeutic and diagnostic applications.

Methods

Sequence alignment and homology modeling

Multiple sequence alignment (the alignment of three or more biological sequences of proteins sharing a common evolutionary origin) between AChBP and the amino-terminal extracellular domain of rat and human α7, and rat and human α4 and β2 nAChR subunits was performed using the Program DCA (Divide-and-Conquer Multiple Sequence Alignment) of the Technical Faculty of the University of Bielefeld (Germany) [24]. Homology modeling is a method for constructing an atomic-resolution 3D model of a protein starting from its amino acid sequence and using as a 3D-target another protein sharing a detectable level of sequence similarity. The 3D-prediction of the amino-terminal extracellular domain of human α7, rat α7, human α4 and human β2 nAChR subunits was performed with the program SwissModel [25–27] using the First Approach Mode with user-defined 3D-templates including energy minimization performed with the program Gromos 96 [28].

For the amino-terminal extracellular domain of human α7, rat α7, human α4, and human β2 subunits, the 3D-templates used were the AChBP monomer [Pdb code=1i9b, 9], the amino-terminal extracellular domain of chick α7, and rat α4 and β2 subunits [29], respectively. The 3D-templates rat α4β2 and chick α7 pentamers were retrieved from the Ligand-Gated Ion Channel database of the Pasteur Institute, France [29].

The 3D models of the pentamer of neuronal rat and human $(\alpha4)_2(\beta2)_3$, rat $(\alpha7)_5$ and human $(\alpha7)_5$ nAChR subtypes were assembled and manually refined, to correct non-allowed geometrical parameters, with the software SYBYL 6.8 (Tripos, St. Louis, MO). All assessment of the geometry of the model was performed using the program PROCHECK [30].

Energy minimization and molecular dynamics

Preparation of the AChBP dimer with acetylcholine in the binding cavity took into account the 3D orientation of N-2-hydroxyethylpiperazine-N′-2-ethane-sulfonate (HEPES). Each binding site of the AChBP pentamer contains a molecule of HEPES coming from the crystallization procedure. Similar to known nicotinic ligands, this buffer molecule has a positively charged nitrogen that stacks onto Trp 143, making the very important cation-π interactions essential for the binding of ligands to nicotinic receptors [31, 32]. Acetylcholine was then inserted into the AChBP binding site by matching the positively quaternary nitrogen with the nitrogen of HEPES involved in the cation-π interaction as shown in Fig. 1. Acetylcholine was param-

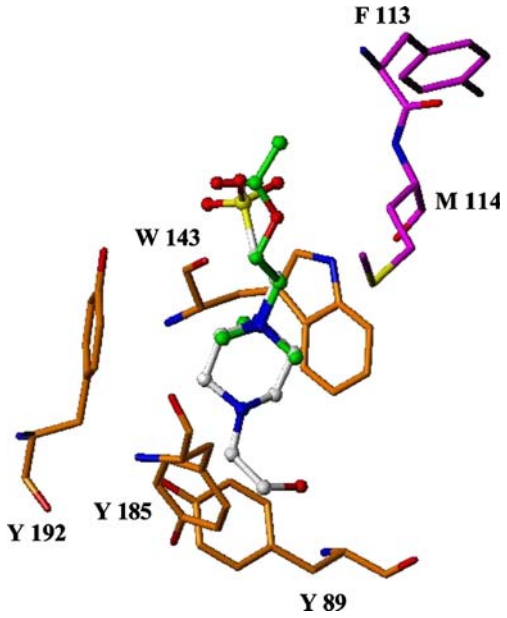

Fig. 1 Binding site region of the acetylcholine-binding protein (AChBP) dimer model. N-2-Hydroxyethylpiperazine-N′-2-ethane-sulfonate (HEPES) from X-ray structure (colored by atom type; *white* carbon atoms) and modeled acetylcholine (colored by atom type; *green* carbon atoms) are displayed in ball and stick mode. Residues of (+)-side and (−)-side are colored by atom type with the carbon atoms in *orange* and *magenta*, respectively. All residues are displayed as *capped sticks* and labeled

eterized using the program ANTECHAMBER. The topology and starting coordinates of the AChBP dimer with acetylcholine in the binding cavity were prepared using LEAP. The same procedure was used to generate 3D models of the pentamer of neuronal rat and human $(\alpha4)_2(\beta2)_3$, rat $(\alpha7)_5$ and human $(\alpha7)_5$ nAChR subtypes and the AChBP pentamer.

All pentamers were immersed in a box of water molecules and Na^+ counterions were added to the solvent bulk of the protein/water complexes to maintain neutrality of the system using program AMBER6 [33].

Periodic boundary conditions were applied. The Amber force field [34] all atom parameters (parm94) were used for the protein and Na^+ ions. The minimization protocol consisted of 1,000 cycles of steepest descent followed by conjugate gradient method until the root-mean square deviation (RMSD) of the Cartesian elements of the gradient reached a value smaller than 0.15 Å.

The dynamic protocol consisted of three steps: MD1, MD2 and MD3. The initial temperatures for MD1, MD2 and MD3 were set at 0, 150, 300°K, respectively, while the targeted temperature during the run was 300°K. The Berendsen's coupling algorithm [35] was applied to keep the temperature constant. The time step for all three dynamic procedures was 0.002 ps. For minimization and MD, the primary cutoff distance for non bonded interaction was set at 9 Å.

Regarding the MD protocol used, the first step (MD1) aimed for the equilibration of water molecules and ions of the water-boxed and charge-neutralized model. An initial velocity was given to the system and trajectories were then allowed to evolve in time according to Newtonian laws, keeping the model protein fixed. The number of dynamics steps was 7,500, corresponding to 15 ps.

Fifteen picoseconds of constant volume dynamic (MD2) was performed on the whole system to adjust the density to a value of 1 atm. In the third step, a 500 ps constant pressure dynamic (MD3) of 1 atm was applied without any constraint to finally assess the stability of the models over time. The energy minimization, MD and corresponding analysis were performed using program AMBER6 [33]. All geometry quality assessment of the models, at different time points, was made using the program PROCHECK [30].

Lipophilicity and electrostatic potential studies

The lipophilicity and electrostatic potential surfaces of AChBP and the rat and human nicotinic models were examined using the program MOLCAD implemented in SYBYL 6.8 [36].

Results and discussion

Sequence alignment and homology modeling

Sequence alignment revealed the identities and homology between AChBP and the amino-terminal extracellular domain of nAChR subtypes human α7, the amino-terminal extracellular domain of chick α7 and rat α7, and the amino-terminal extracellular domains of rat α4, rat β2 and human α4, human β2; percentage identities are shown in Table 1. There is high homology between the same nicotinic

Table 1 Percentage of sequence identities between acetylcholine-binding protein (AChBP) and the amino-terminal extracellular domain of nicotinic acetylcholine receptor (nAChR) subtypes human α7, the amino-terminal extracellular domain of chick α7 and rat α7, and the amino-terminal extracellular domains of rat α4, rat β2 and human α4, human β2 computed with the LALIGN program [40]

	Template				
		AChBP	α 7c	α 4r	β 2r
Target[a]	AChBP	100	27.8	25.8	22
	α 7h	28.8	93.7	44.9	40
	α 7r	28.3	91.2	45.4	39.9
	α 4h	24.9	45.9	97.6	53.4
	β 2h	24.6	40.4	54.3	98.5

[a] Lower case letters *c*, *r* and *h* indicate chick, rat and human, respectively

subtypes of different species, confirming a common point of origin during the evolution of the ligand-gated ionic channel superfamily [37].

The AChBP homopentamer has five binding sites. Each binding site is formed in a cleft made of different loops, part of the principal subunit face (plus side), a series of β-strands, and part of the complementary adjacent subunit face (minus side) [9]. The plus/minus side interface is formed by amino acids Tyr 89 (loop A), Trp 143, Thr 144, His 145 (loop B), Tyr 185, double Cys 187,188 and Tyr 192 (loop C), all belonging to the plus side, and the minus side amino acids Trp 53, Gln 55 (β-strand D), Leu 112, Met 114 (β-strand E). Within this interface, a cavity with a top (Tyr 89, Tyr 185, Tyr 164, Trp 53), a bottom (Leu 112) and walls (Tyr 192, Trp 143, the main chain closed to His 145, the side chains of Met 114, Gln 55, double Cys 187,188) is formed [9]. The aromatic residues Tyr 89, Trp 143, Tyr 192 of the plus side and Trp 53 of the minus side are involved in cation-π interactions with HEPES and acetylcholine as shown in Fig. 1 [9]. At the residue level, the homology of the four nicotinic models with AChBP involves the plus side more than the minus side, as shown in Table 2. The AChBP aromatic residues Tyr 89, 192 and Trp 143 of the plus side, and Trp 53 of the minus side are conserved and maintain a similar 3D-orientation in all α and β subunits of different species (Fig. 2). The residues Arg 104, Val 106, Leu 112, Met 114, which form the minus side of AChBP, are poorly conserved within the different nicotinic subunits (Table 2). In the binding site region of the rat $(\alpha4)_2(\beta2)_3$ model, the residues expected to be involved in ligand binding are on the α subunit Tyr 91 (loop A), Trp 147 (loop B), Tyr 188, double Cys 190,191, Tyr 195 (loop C) and, on the β subunit, Trp 55, Thr 57 (β-strand D), Val 109, Ser 111, Phe 117, Leu 119 (β-strand E). The residues involved in binding are highly conserved between the rat and human models. If we compare the neuronal α4β2 and α7 subtypes of the same species, high homology is present mostly between the α-subunits (Tables 1, 2). Residues on the α-subunit (plus side) are conserved within different subunits of the same species and within the same subunit of different species, confirming the findings of Le Novère et al. with the chick $(\alpha7)_5$ model [29]. While the plus side is the principal component involved in ligand binding in the interface of adjacent subunits [1], the minus side behaves as the complementary component and may be the side responsible for subtype specificity. In fact, the complementary minus side appears to be less conserved, and to have the capacity

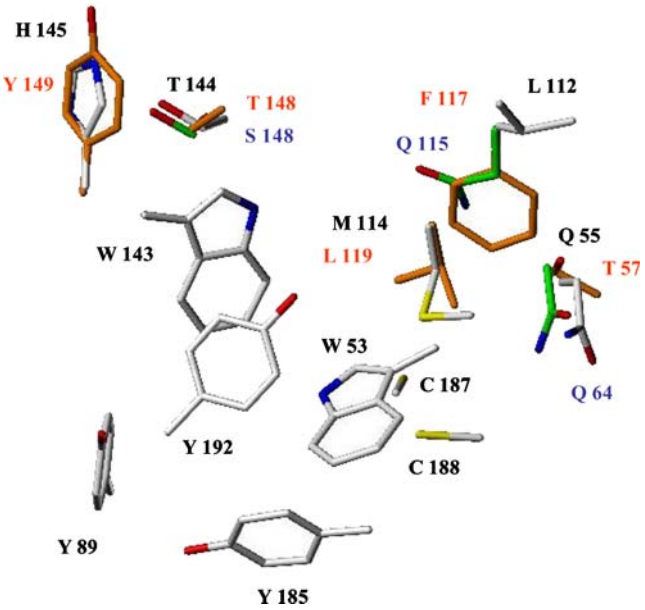

Fig. 2 Superimposition of the binding site of AChBP (colored by atom type; *white* carbon atoms), the rat (α4β2) pentamer model (colored by atom type; *orange* carbon atoms), and the rat (α7) pentamer model (colored by atom type; *green* carbon atoms). The residues are labeled *black* (AChBP), *red* (α4β2) and *blue* (α7). In the case of residue conservation within the three models, or within the rat (α4β2) and (α7) models, only the AChBP amino acid side chain or the AChBP and rat (α4β2)amino acid side chains are shown, respectively. All side chains residues are displayed as *capped sticks*

Table 2 Residue homology between AChBP and the different nicotinic subtype models at the level of the 3D-structure. *C* Cys, *F* Phe, *H* His, *L* Leu, *M* Met, *Q* Gln, *S* Ser, *T* Thr, *V* Val, *Y* Tyr, *W* Trp

Residue												
Model[a]	α-subunit								β- or α-subunit (for α7)			
AChBP	Y_{89}[a]	W_{143}	T_{144}	H_{145}	Y_{185}	C_{187}	C_{188}	Y_{192}	W_{53}	Q_{55}	L_{112}	M_{114}
α4β2r	Y_{91}	W_{147}	T_{148}	Y_{149}	Y_{188}	C_{190}	C_{191}	Y_{195}	W_{55}	T_{57}	F_{117}	L_{119}
α4β2h	Y_{91}	W_{147}	T_{148}	Y_{149}	Y_{188}	C_{190}	C_{191}	Y_{195}	W_{55}	T_{57}	F_{117}	L_{119}
α7r	Y_{91}	W_{147}	S_{148}	Y_{149}	Y_{186}	C_{188}	C_{189}	Y_{193}	W_{58}	Q_{64}	Q_{115}	L_{117}
α7h	Y_{91}	W_{147}	S_{148}	Y_{149}	Y_{186}	C_{188}	C_{189}	Y_{193}	W_{58}	Q_{64}	Q_{115}	L_{117}
	(+)-Side								(−)-Side			

[a] Residues are numbered based on the Swissprot sequences
[a] Lower case letters *r* and *h* indicate rat and human, respectively

of adopting a number of different conformations. In contrast, the plus side is fairly rigid, especially in the bound-state conformation with the exception of some ring flipping of the tyrosines [20].

In the α4β2 and α7 nicotinic models, the homologues of the conserved aromatic residues Trp 143, Tyr 89, 185 and 192 (plus side) and Trp 53 (minus side) of AChBP form, on different loops, a hydrophobic pocket in the inner part of the cavity, which is amenable to cation-π interactions (Fig. 1) [19]. On the other hand, the homologues of the poorly conserved residues Gln 55, Leu 112 and Met 114 (minus side) of AChBP are on different β-sheets and cover this aromatic pocket (Fig. 2). These residues are more involved in hydrogen bonds between their main chain amides and the ligand [20]. According to Henchman et al. [19] hydrophobic interactions also contribute to the binding of ACh to the minus side of the α7 nAChR subtype. The ACh binding site is located at the interface between two subunits, and the ligand must penetrate into a gorge to interact specifically with the receptor and give the biological response [19]. The double-cysteine loop seems to be located, as in AChBP, at the entrance of the cavity regulating access to the binding cavity [19–21].

Molecular dynamics

The AChBP pentamer and the AChBP dimer with acetylcholine were submitted to the described minimization and MD protocol. The RMSD of the AChBP pentamer and dimer as a function of time clearly shows that a plateau, representing stable conformation over time, was reached already after 100 ps (Fig. 3). Moreover, comparison of the structures at different times of MD with the starting structure revealed no major changes in overall conformation. The low RMSD (1.5 Å) and structural comparison along the simulation time indicates that, as expected, the starting X-ray structure represents a stable conformation, and that the MD protocol is well suited to assessing the stability of the models.

The rat and human $(\alpha4)_2(\beta2)_3$, and rat $(\alpha7)_5$ and human $(\alpha7)_2$ models were submitted to the same MD protocol to assess their stability. The RMSD graphics versus time are shown in Fig. 3. The RMSD profile clearly shows that all molecules reached a plateau and thus conformational stability. As expected, the RMSD values of the nicotinic models were found to be higher between 2.5 and 3 Å than the values of the crystal structure AChBP.

The AChBP dimer complexed with acetylcholine was investigated. The MD and the subsequent analysis of the structure at different times revealed that the cation-π interaction is stable over time. A low RMSD value of around 1.3 Å was found, and conformational stability was reached already after 50 ps. This is in agreement with the importance of cation-π interactions in the binding of ligands to nicotinic receptors, as shown by site-directed mutagenesis of residues Tyr 93, Trp 149, Tyr 188, Tyr 195 and Trp 55 of the α7 nAChR subtype [36]. Point mutations of these hydrophobic residues to alanine leads to dramatically impaired binding properties of the agonists and antagonists studied [38].

In the case of the AChBP dimer without acetylcholine, Trp 143 (loop B) and Tyr 192 (loop C) shift toward the inner of the cavity during MD, while in the AChBP dimer with acetylcholine, Trp 143 and Tyr 192 do not show a significant shift. Hence, this suggests that the observed shift is due to the dynamic, although the movement of Trp 143 and Tyr 192 toward the inside of the binding cavity is strictly dependent on the emptiness of the cavity itself. In

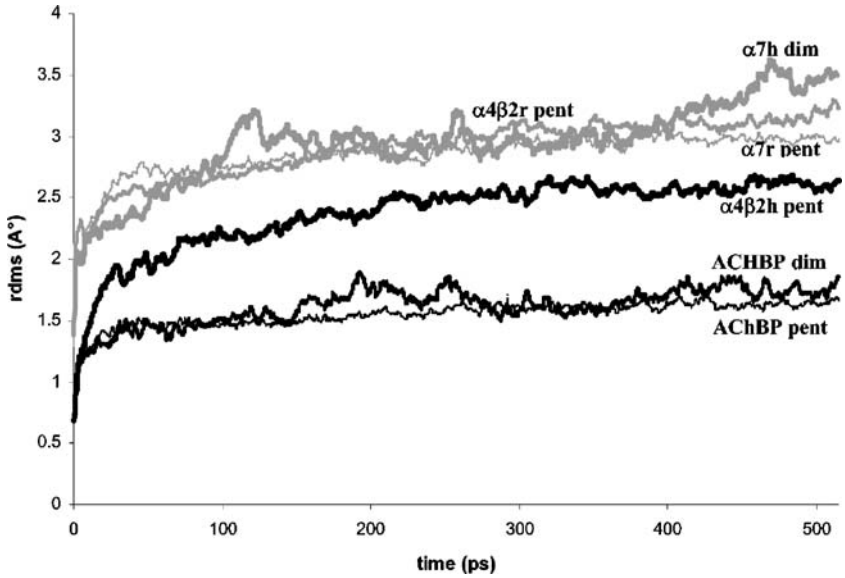

Fig. 3 Root-mean square deviation (RMSD) graphics (all atoms plotted) versus time (picoseconds). The observed increase in RMSD after 400 ps with the human α7 dimer can be expected due to the fragility of a dimer model submitted to lengthy dynamics

fact, looking at the empty binding site region of rat and human $(\alpha4)_2(\beta2)_3$, rat $(\alpha7)_5$ and human $(\alpha7)_2$ models after dynamics, we noted the same positional shift of the Trp and Tyr residues—both conserved residues within the different nicotinic α-subunits. A similar shift of Trp 148 in the middle of the binding site was also observed by Henchman et al. [19] during MD simulations of the α7 nAChR-LBD. In the absence of the ligand, the binding site seems more collapsed than when the ligand is bound, and this was well quantified by following up the distance Cys 189–Leu 118 during the simulation period [19].

Lipophilicity and electropotential studies

Examination of the lipophilicity surface of AChBP and of the rat and human α4β2 and α7 nicotinic models (Fig. 4) revealed the polarity of the outer surface of the protein, which is more exposed to the solvent, and the clear visible hydrophobicity of the binding cavity. Inside the binding cavity, the hydrophobic region involves primarily the aromatic pocket composed of AChBP plus side residues Trp 143, Tyr 89, 185 and 192 and the corresponding residues (Table 2) in the α-subunit of the α4β2 and α7 nicotinic models. As shown in Fig. 4a and b, the hydrophobic region of the rat α7 nicotinic model is larger than that of the rat α4β2, involving a bigger portion of the binding cavity surface. This would favor stronger interactions between the binding site and the hydrophobic moieties of ligands. The aromatic residues forming the hydrophobic pocket establish cation-π interactions with the positively charged nitrogen of the ligand [9, 39]. The minus side of AChBP and the nicotinic models is less hydrophobic, suggesting the possibility of a different type of binding to the ligand.

The lipophilicity surface of both human models is similar to the rat models, revealing an outer hydrophilic surface and an inner hydrophobic binding cavity. The difference in lipophilicity between the α7 and α4β2 models (higher for the α7 model) is present in both rat and human nicotinic subtypes (Fig. 4c,d). With the human

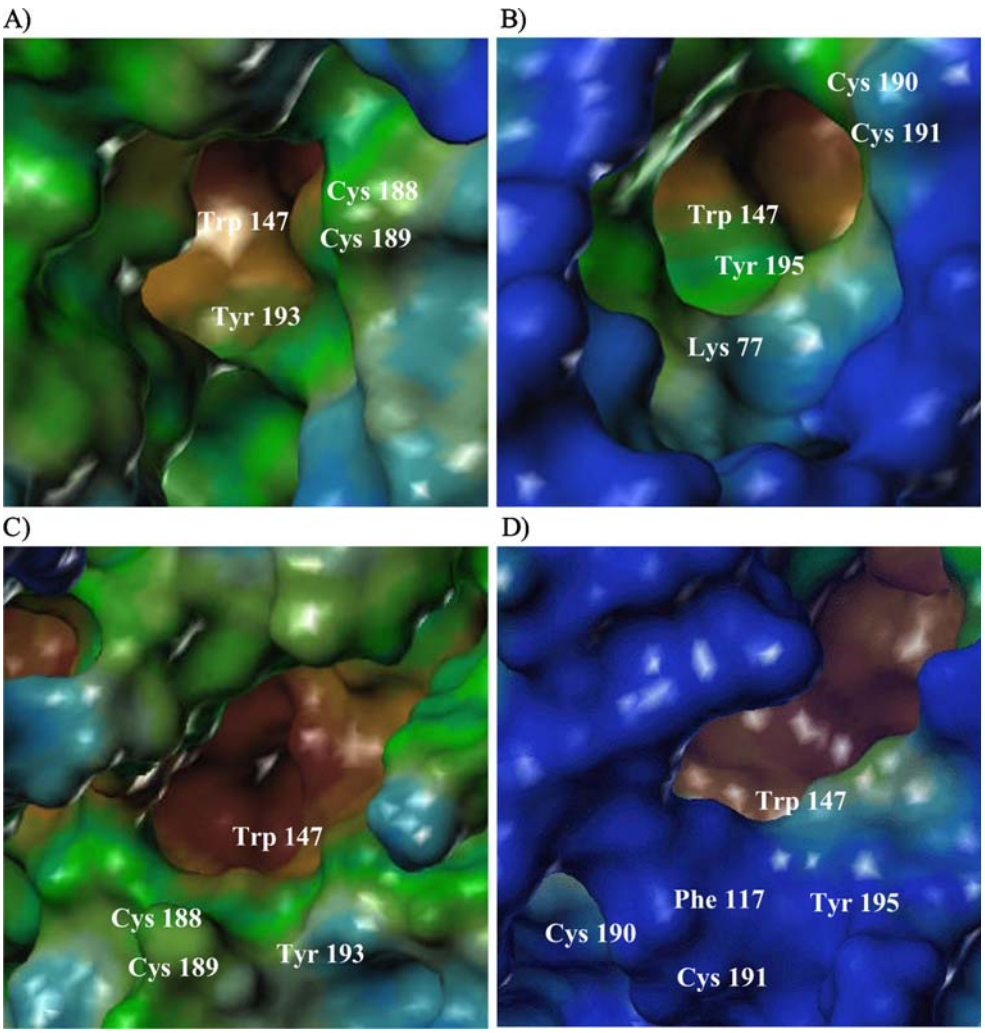

Fig. 4 Lipophilic surface of the X-ray structure of the AChBP dimer of the binding site cavity of the rat α7 (**a**) and α4β2 (**b**), and human α7 (**c**) and α4β2 (**d**) nicotinic model performed with the MOLCAD program. All residues labeled are part of the α7 (**a**,**c**) and α4 (**b**,**d**) subunit, with the exception of Phe 117, which is part of subunit β2 (**d**). *Brown* Hydrophobic, *grey* slight hydrophobic, *green* neutral, *blue* hydrophilic

models, we also confirmed that the plus side of the binding site is more lipophilic than the minus side. This means that the interpretation of the rat models can also be applied to the human models. The plus side is involved in cation-π interactions with the ligand [9, 19, 20, 38], while the minus side, due to its lower hydrophobicity, may be involved in another type of binding to the ligand. Moreover, the plus side hydrophobic residues Trp 143, Tyr 185 and Tyr 192 are structurally part of loop C of the LBD, movement of which upon binding of an agonist or antagonist is connected with the opening (active state) or the closing (inactive/resting state), respectively, of the ion channel pore via TMD-M1 [18].

Investigation of the electrostatic potential of the binding cavity of AChBP revealed a negatively charged surface surrounding Trp 143, which attracts positively charged ligands. Similar results were obtained with the rat α4β2 and α7 nicotinic models (Fig. 5a,b). The negatively charged area surrounding Trp 147 is present in both models but, in the rat α4β2 model, it is larger and involves also Tyr 195 (Fig. 5a,b). In the rat α4β2 model, the distance between Trp 147 and Tyr 195 is smaller (0.2–0.4 Å) than the homologous residues in the rat α7 model. This means that, of the two rat models, the α4β2 binding site region is more capable of attracting and stabilizing positively charged ligands deep inside the cavity. Another difference between the two rat models is the role of α4β2-Lys 77 on the β2-subunit. This residue showed a neutral electrostatic potential and a 3D location that would favor interaction with hydrogen bonding acceptors of the ligand, as we also observed in our docking studies with the α4β2 nAChR subtype [39], whereas the homologous residue Lys 72 in the α7 3D model is located further from the binding cavity, making its involvement during ligand binding less probable.

The electrostatic potential studies revealed that the human α7 and α4β2 models are less negatively charged in the binding site region (especially the minus side electrostatic potential surface) than the rat models (Fig. 5c,d). Moreover, the α7 residue Tyr 193 is involved

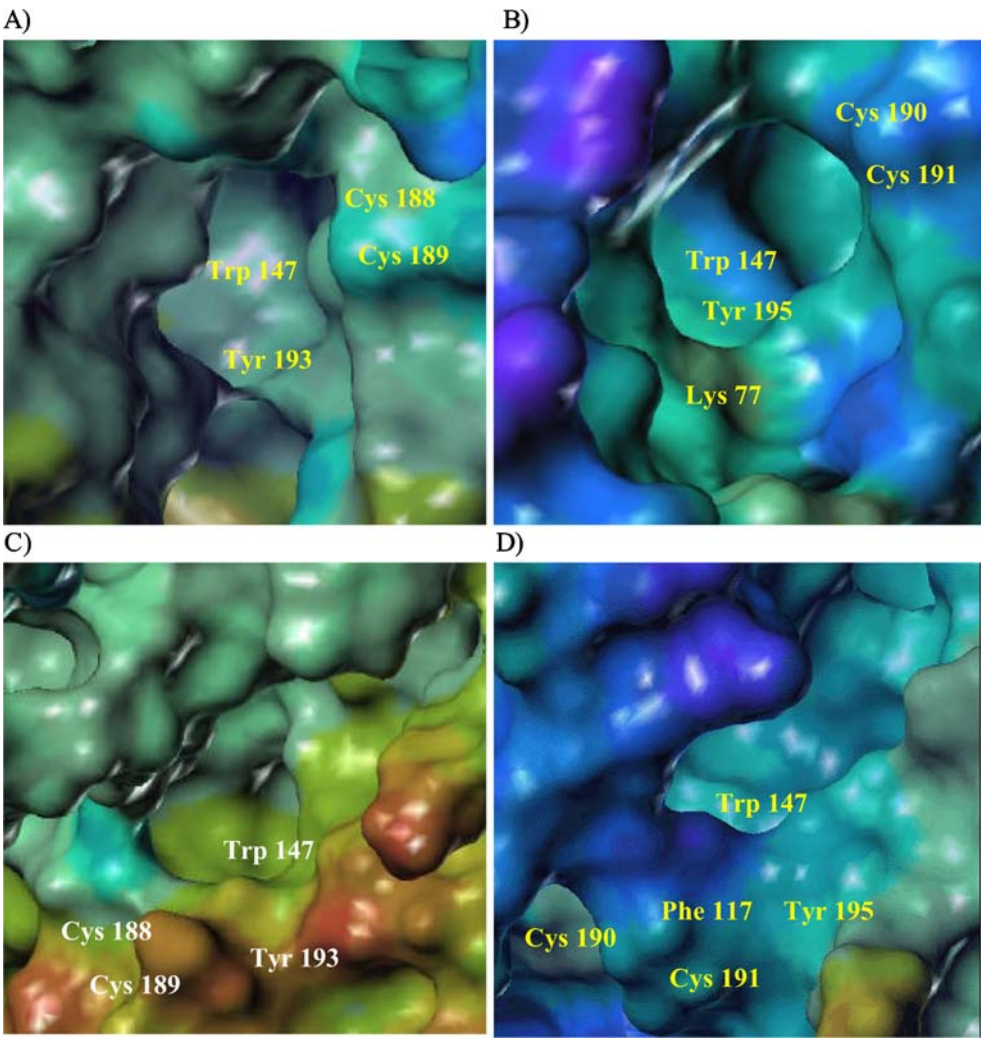

Fig. 5 Electrostatic surface potential of the binding site cavity of nAChR. Nicotinic models performed with the MOLCAD program: **a** rat α7, **b** rat α4β2, **c** human α7, **d** human α4β2. All residues labeled are part of the α7 (**a**,**c**) or α4 (**b**,**d**) subunit with the exception of Phe 117, which belongs to subunit β2 (**d**). *Violet* Very negative, *blue* negative, *yellow* neutral, *red* very positive

with less extension in the human than in the rat model. This is due to the 3D-shift of the phenyl ring of Tyr towards Trp 147, which causes less exposure of the phenyl negatively charged surface of Tyr 193 in the binding cavity (Fig. 5c). Instead, in the human α4β2 model, the 3D-orientation of Trp 147 and Tyr 195 is similar to that of the rat α4β2 model (the two residues are slightly closer in the rat model) as shown in Fig. 5d.

A significant difference between the rat and human α4β2 models is found by looking at the entrance to the binding cavity. Due to the 3D orientation of Phe 117 in the human model, the cavity entrance is shifted so that it differs from that found in the rat model (Fig. 5d). Consequently, in the α4β2 human model, the ligand will have to enter the binding cavity in a different way than in the rat model. While the kinetics of binding may be different because of the peculiarity of the entrance, it is expected that the binding orientation of acetylcholine in the binding site will be similar because of the conservation of this major ligand-receptor in both human models as well as the rat models. This is due to the fact that the rat and human binding sites of the same subtype share high similarities (>90%) at both the level of subunit sequence (Table 2) and 3D binding pocket structure. The differences between subtype binding sites of the same species are important in investigating subtype specificity, and in our case neuronal specificity, because α7 and α4β2 are the subtypes most abundant in the brain. The present lipophilic and electrostatic potential surface analysis highlights a major feature: due to differences in the 3D orientation of the residues involved in binding, the α4β2 binding site is less lipophilic and shows a bigger negative potential area around Trp 147 than the α7 subtype. Similar data were obtained with both rat and human models. Thus, this allows us to discriminate the two binding sites and, as a consequence, suggests the possibility of designing specific α4β2 nAChR subtype ligands.

Summary

The high homology between the different nicotinic subunits from different species has allowed us to build models of the extracellular domain of rat and human $(\alpha4)_2(\beta2)_3$ and $(\alpha7)_5$ nicotinic receptor subtypes, which are the most abundant subtypes in the brain. These models were successfully assessed using molecular dynamics and show conformational stability over time.

Lipophilicity and electrostatic potential surface analyses of the rat and human α4β2 and α7 nicotinic models compared to AChBP revealed, for both species, the importance of the hydrophobic aromatic pocket and the critical role of the α-subunit Trp—the homologue of AChBP Trp 143—for ligand binding. Moreover, due to differences in the 3D orientation of the residues involved in binding, the α4β2 binding site in both species shows minor lipophilicity and a bigger negative potential area around Trp 147 than the α7 subtype.

These models, which reveal differences between α7 and α4β2 subtypes of the same species as well as the high similarity between the same subtype of different species (rat vs human in our case), will be useful as a valuable framework for structure-based design of specific α4β2 nAChR subtype ligands aimed at improving human therapeutic and diagnostic applications involving this cationic channel receptor.

References

1. Karlin A (2002) Nat Rev Neurosci 3:102–114
2. Sine SM, Engel AG (2006) Nature 440:448–455
3. Badio B, Daly JW (1994) Mol Pharmacol 45:563–569
4. Arneric SP, Holladay M, Williams M (2007) Biochem Pharmacol 74:1092–1101
5. Itièr V, Bertrand D (2001) FEBS Lett 504:118–125
6. Hogg R, Bertrand D (2003) Drug News Perspect 16:261–266
7. Miyazawa A, Fujiyoshi Y, Unwin N (2003) Nature 423:949–955
8. Unwin NJ (2005) Mol Biol 346:967–989
9. Brejc K, Van Dijk WJ, Klaassen RV, Schuurmans M, Van der Oost J, Smit AB, Sixma TK (2001) Nature 411:269–276
10. Sixma TK, Smit AB (2003) Annu Rev Biophys Struct 32:311–334
11. Celie PH, van Rossum-Fikkert SE, Van Dijk WJ, Brejc K, Smit AB, Sixma TK (2004) Neuron 41:907–914
12. Celie PH, Kasheverov IE, Mordvintsev DY, Hogg RC, van Nierop P, van Elk R, van Rossum-Fikkert SE, Zhmak MN, Bertrand D, Tselin V, Sixma TK, Smit AB (2005) Nat Struct Mol Biol 12:582–588
13. Taylor P, Talley TT, Radic Z, Hansen SB, Hibbs RE, Shi J (2007) Biochem Pharmacol 74:1164–1171
14. Harel M, Kasher R, Nicolas A, Guss JM, Balass M, Fridkin M, Smit AB, Brejc K, Sixma TK, Katchalski-Katzir E, Sussman JL, Fuchs S (2001) Neuron 32:265–275
15. Hansen SB, Radic Z, Talley TT, Molles BE, Deerinck T, Tsigelny I, Taylor P (2002) J Biol Chem 277:41299–41302
16. Hansen SB, Radic Z, Talley TT, Taylor P (2003) Faseb J 17: A641–A641
17. Hansen SB, Talley TT, Radic Z, Taylor P (2004) J Biol Chem 279:24197–24202
18. Law RJ, Henchman RH, McCammon JA (2005) Proc Natl Acad Sci USA 102:6813–6818
19. Henchman RH, Wang H-L, Sine SM, Taylor P, McCammon JA (2005) Biophys J 88:2564–2576
20. Zhang D, Gullingsrud J, McCammon JA (2006) J Am Chem Soc 128:3019–3026
21. Taly A, Corringer P-J, Grutter T, de Carvalho LP, Karplus M, Changeux JP (2006) Proc Natl Acad Sci USA 103:16965–16970
22. Szarecka A, Xu Y, Tang P (2007) Proteins 68:948–960
23. Amiri S, Sansom MSP, Biggin PC (2007) Protein Eng Des Sel 20:353–359
24. Stoye J (1998) Gene 211:45–56
25. Guex N, Peitsch MC (1997) Electrophoresis 18:2714–2723
26. Peitsch MC (1996) Biochem Soc Trans 24:274–279
27. Peitsch MC (1995) Biotechnology 13:658–660
28. http://igc.ethz.ch/gromos

29. Le Novère N, Grutter T, Changeux JP (2002) Proc Natl Acad Sci USA 99:3210–3215
30. Laskowski RA, MacArthur MW, Moss DS, Thornton JM (1993) J Appl Crystallogr 26:283–291
31. Zhong W, Gallivan JP, Zhang Y, Li L, Lester HA, Dougherty DA (1998) Proc Natl Acad Sci USA 95:12088–12093
32. Schmitt JD, Sharples CGV, Caldwell WS (1999) J Med Chem 42:3066–3074
33. http://amber.scripps.edu/doc6/amber6.pdf
34. Cornell WD, Cieplak P, Bayly CI, Gould IR, Merz KM, Ferguson DM, Spellmeyer DC, Fox T, Caldwell JW, Kollman PA (1995) J Am Chem Soc 117:5179–5197
35. Berendsen HJC, Postma JPM, van Gunsteren WF, DiNola A, Haak JRJ (1984) Chem Phys 81:3684–3690
36. Brickmann J, Goetze T, Heiden W, Moeckel G, Reiling S, Vollhardt H, Zachmann C-D (1995) Data visualization in molecular science: tools for insight and innovation. Addison-Wesley, Reading, MA
37. Lukas RJ (1998) The nicotinic acetylcholine receptor: current views and future trends. Springer, Berlin
38. Jensen AA, Zlotos DP, Liljefors TJ (2007) J Med Chem 50:4616–4629
39. Bisson WH, Scapozza L, Westera G, Mu L, Schubiger PA (2005) J Med Chem 48:5123–5130
40. Huang X, Miller W (1991) Adv Appl Math 12:373–381